FOSSEE, IIT Bombay
OpenFOAM Case Study Project
June 2024

Aerodynamics of Bristled Wings

Yukesh Karki[1] and Chandan Bose[2]

[1]UG Research Scholar, Dept. of Mechanical and Aerospace Engineering, Tribhuvan University, IOE, Pulchowk Campus
[2]Assistant Professor, Aerospace Engineering, College of Engineering and Physical Sciences, The University of Birmingham

July 23, 2024

Synopsis

Microscopic flying insects like thrips and fairyflies possess a distinct wing structure characterized by several bristles extending from a main frame. At low Reynolds numbers of $O(10)$, bristled wings exhibit enhanced aerodynamic efficiency compared to solid membranous wings. This study presents a numerical investigation of bristled wing models at two different angles of attack and a Reynolds number of 30 using the open-source computational fluid dynamics (CFD) package OpenFOAM. Three bristled wing geometries with 4, 5 and 6 bristles were examined. Results indicate that force coefficients increased with the number of bristles, while decreasing gap width between bristles minimized flow leakage through strong viscous diffusion, creating a virtual fluid barrier resulting it to act like a membranous wing. Among the studied bristled wing models, the 6-bristled wing model demonstrated comparable drag to the solid wing model despite its smaller surface area. However, achieving an optimal bristled wing configuration requires a systematic investigation comparing various wing models with different bristle numbers based on generated lift, drag, lift-to-drag ratio, and other parameters.

1 Introduction

Microscopic insects like thrips and fairyflies, measuring 300 to 1000 microns in length, have long puzzled scientists with their ability to fly. Initially, it was believed that they merely drifted with the wind. However, recent studies have shown that these tiny insects can fly very well, displaying great maneuverability in the air. To sustain flight, these insects must generate enough lift to counteract their entire body weight. Previous research conducted by Santhanakrishnan et. al. [1] demonstrated that when a solid elliptical wing maintains a constant revolution at a steady angle of attack, drag experiences a substantial increase with decreasing Reynolds number, while the increase in lift appears to be minimal as illustrated in Figure 1.

In order to overcome the challenge posed by these heightened drag forces, microscopic insects have evolved bristled wings [2–5]. Bristled wings consist of multiple cylindrical bristles extending

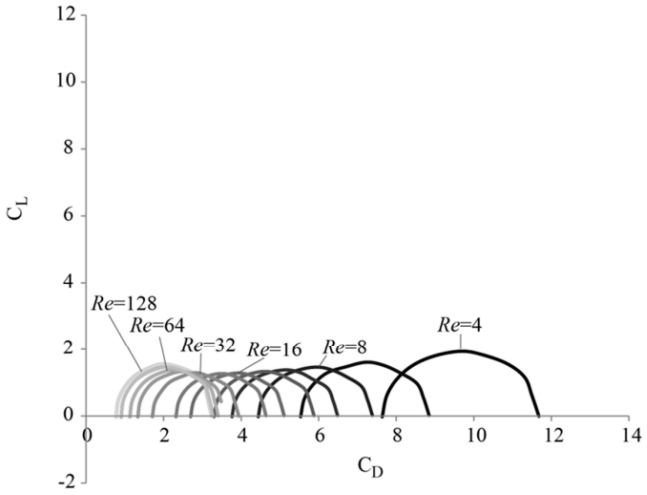

Figure 1: C_l vs C_d for over a range of Re [1].

from a main frame, creating a discontinuous surface with gaps between the bristles as can be seen in figure presented in the work of Huber et. al. [6]. The simplified 2D representation of a bristled wing is shown in Figure 2. At high Reynolds numbers, the array demonstrates rake-like behavior. However at very low Reynolds numbers, the array of hairs behaves like paddles, with minimal fluid leakage between them.

Figure 2: 2D birstle wing model [5].

Sunada et. al. [7] conducted experimental research on solid and bristled wing model. They showed that the hairy structure of bristle wing can exert fluid-dynamic forces comparable to those of equivalent solid wing, thus reducing the mass of an insect. Similary, Lee et. al. [8] conducted experiments on comb-like plate, focusing on viscous diffusion. At a low Reynolds number of $O(10)$, shear layers generated at the tooth edges diffused stronlgy blocking the gaps between the teeths. This blockage increased the effective surface area of the plate, altering the formation of leading and trailing edge vortices and resulting in larger aerodynamic forces. Lee et al. [3] numerically investigated the optimal configuration of 2D bristled wings, adjusting the Reynolds number based on bristle diameter (Re_b) and gap width between the bristles. Similar to previous studies, they showed that the flow blockage was increased with decreasing Re_b and decreased with increasing

gap width. Additionally, Lee et al. [2] performed a 2D numerical study on bristled wing models to examine gap flow formation during unsteady deceleration and stroke reversal. In the study conducted by Wu et. al. [5], the drag production mechanism was studied for solid wing and bristled wing. When the bristle number reached a certain value, they showed that there is little to no effect on force production with further increase in bristles with the disadvantage of increasing mass.

In the present study, the flow structure on bristled wing model with 4, 5 and 6 numbers of bristle is numerically investigated at the Reynolds number of 30 based on chord length and compared it with the equivalent solid wing having same aspect ratio. By varying the number of bristles, the aerodynamic performance based on flow structure is evaluated as the gap width between the bristles changes. Two different angle of attack of 90°and 45°is also taken into account for this study to investigate the nature of flow structure and its aerodynamic performance due to changing angle of attack.

2 Governing Equations and Models

2.1 Problem definition

This study investigates the aerodynamic performance of a bristled wing model compared to a solid wing at a Reynolds number of 30 using 2D numerical simulations. This project aims to analyze the influence of bristles on lift, drag and flow phenomena through simulations to evaluate their potential for improved flight performance.

Three bristle wing models are considered with 4, 5 and 6 number of bristles having bristle diameter 10% of L (where L is the chord length of the wing). The equivalent solid wing is also considered for comparison having thickness same as that of the bristle diameter (i.e. 10% of L) with semi-circular leading and trailing edges as seen in Figure 3.

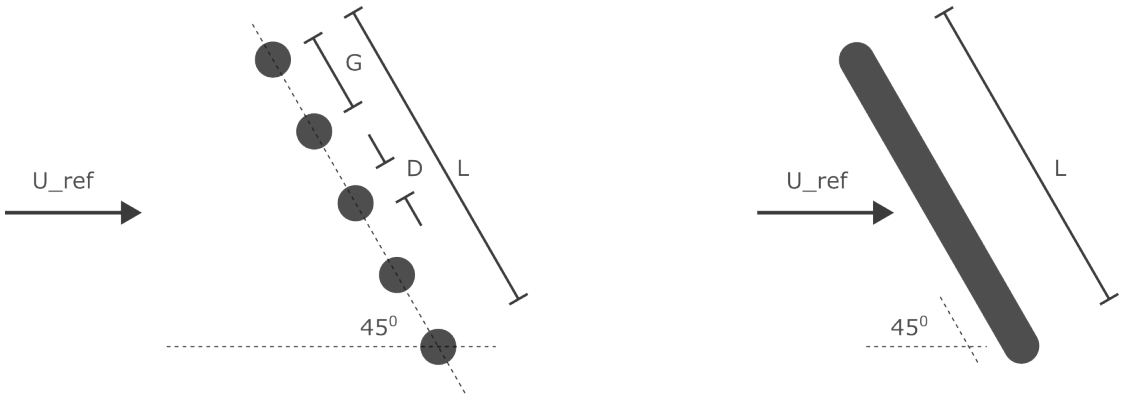

Figure 3: Schematic diagrams of bristled wing model (left) and corresponding solid wing model (right)

2.2 Governing equations

The governing equations for the flows around the model wing are the incompressible Navier-Stokes equations.

Continuity Equation:

$$\nabla \cdot \mathbf{u} = 0 \tag{1}$$

Momentum Equation:

$$\frac{\partial \mathbf{u}}{\partial t} + \mathbf{u} \cdot (\nabla \cdot \mathbf{u}) = -\frac{1}{\rho}(\nabla \cdot p) + \nu \nabla^{\mathbf{2}} \cdot \mathbf{u} \tag{2}$$

where ρ is the density, ν is the kinematic viscosity, $\mathbf{u}$ is the velocity vector and p is the pressure. pimpleFoam , a pressure-based transient, incompressible solver is selected for this study. It employs the PIMPLE algorithm, which combines PISO and SIMPLE methods for pressure-momentum coupling. Turbulence modelling is not performed due to the laminar nature of the flow.

2.3 Geometry and Mesh

blockMesh utility, OpenFOAM's built-in tool, is used to model and discretize the geometry.

2.3.1 Bristle Wing

The computational domain consists 391 vertices and 169 blocks for the domain with 5 bristles wing model. The schematic diagram of the computational domain is shown in Figure 4 and the bristled wing parameters are given in Table 1. The G/D ratio for 4, 5 and 6 number of bristles wing model are 3.33, 2.5 and 2 respectively.

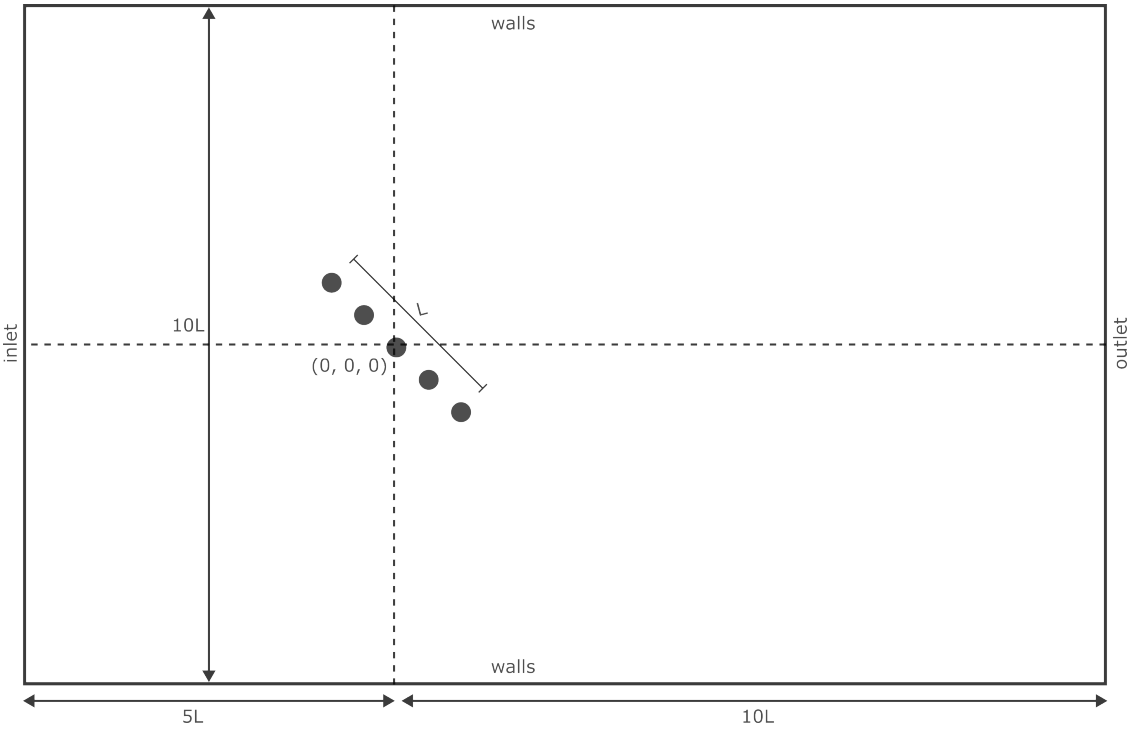

Figure 4: Computational Domain

The computational domain with dimensions of 15L in stream wise direction (-5 < x/L < 10), and 10L in normal direction (-5 < x/L < 5) with the center of wing as origin is adapted in this study.

Table 1: Parameters for 5-Bristled Wing Model

Parameters	Value	Unit
Chord Length (L)	1	meter
Diameter of bristles (D)	0.1	meter
Gap width (G)	0.25	meter

A grid convergence test was conducted to finalize the grid size, as detailed in Section 3.1. The converged mesh has 73,705 hexahedral elements, shown in Figure 5.

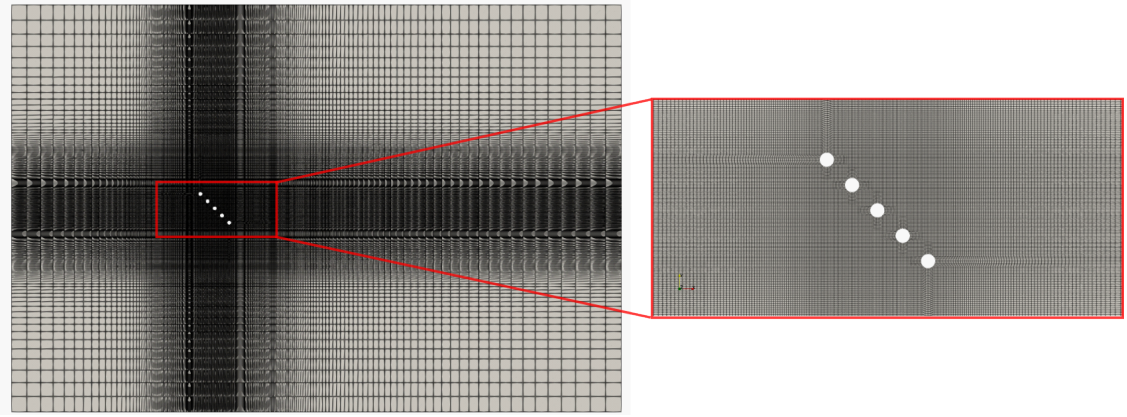

Figure 5: Computational Mesh for bristled wing at 45°AOA

The same converged mesh sizing is used for geometries with 4 and 6 number of bristles as shown in Figure 6 and 7.

Similarly, using the same converged mesh parameters, the mesh is created for geometry with 90°AOA shown in Figure 8, 9 and 10.

2.3.2 Solid Wing

Similar domain was created for solid wing with equivalent chord length. The computational domain consists 89 vertices and 34 blocks. The converged mesh has 43608 hexahedral elements, shown in Figure 11.

Similarly, the mesh created for geometry with 90°AOA is shown in Figure 12.

2.4 Solver setup

The 2D incompressible laminar flow around a bristle wing model is solved numerically using OpenFOAM v2112.

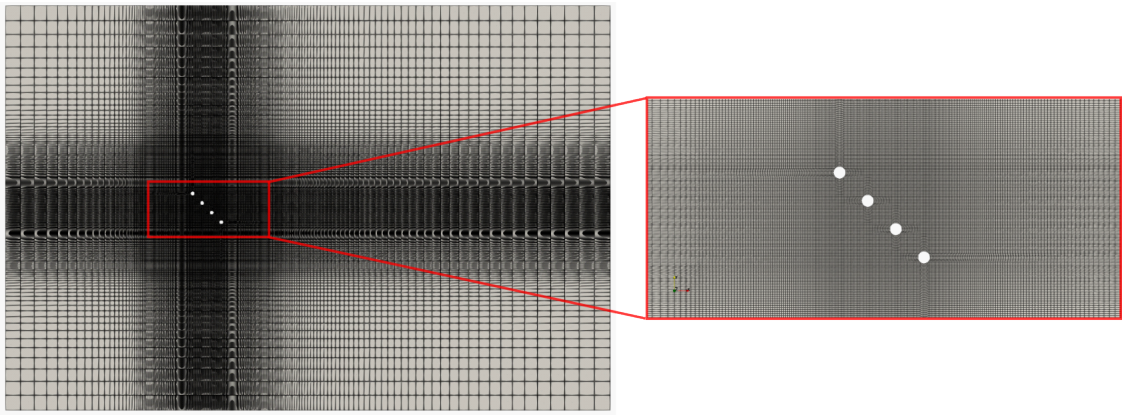

Figure 6: Computational Mesh for 4 bristled wing model at 45°AOA

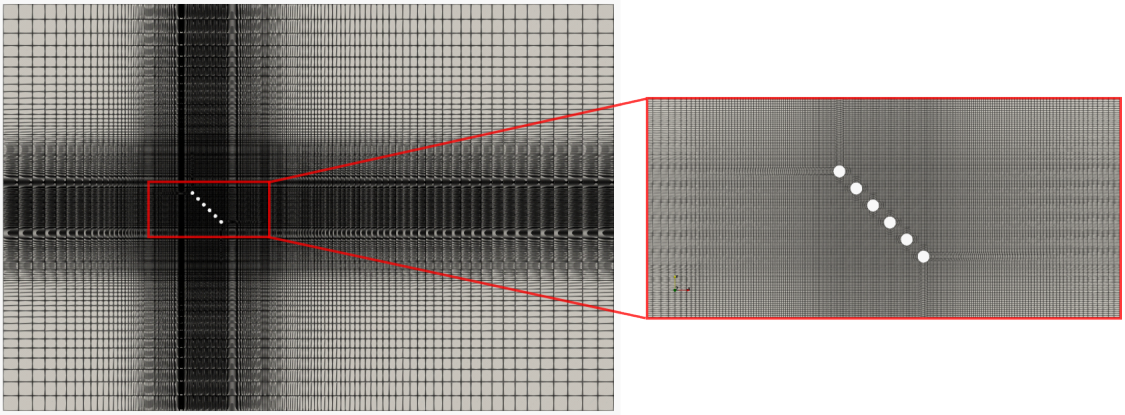

Figure 7: Computational Mesh for 6 bristled wing model at 45°AOA

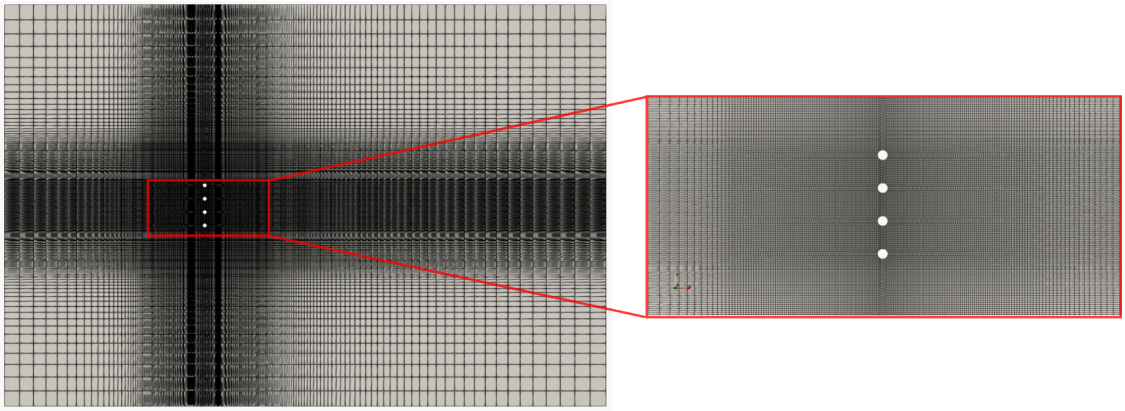

Figure 8: Computational Mesh for 4 bristled wing at 90°AOA

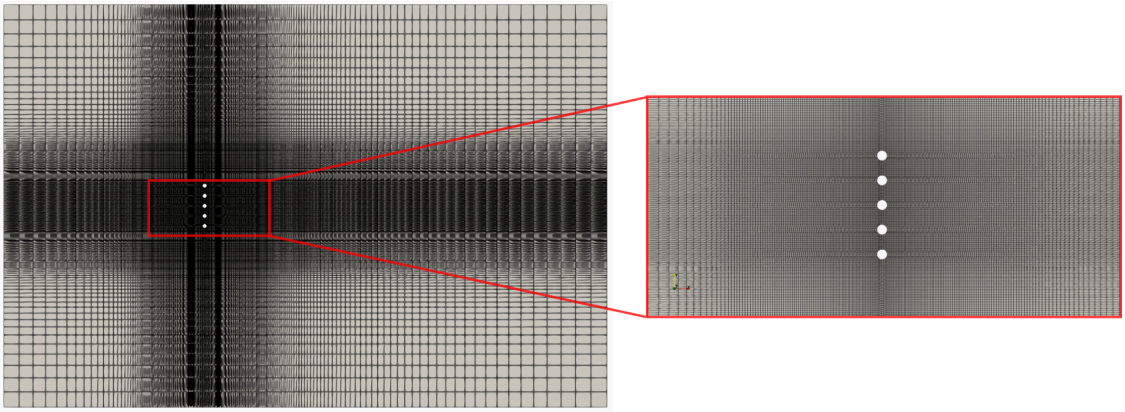

Figure 9: Computational Mesh for 5 bristled wing at 90°AOA

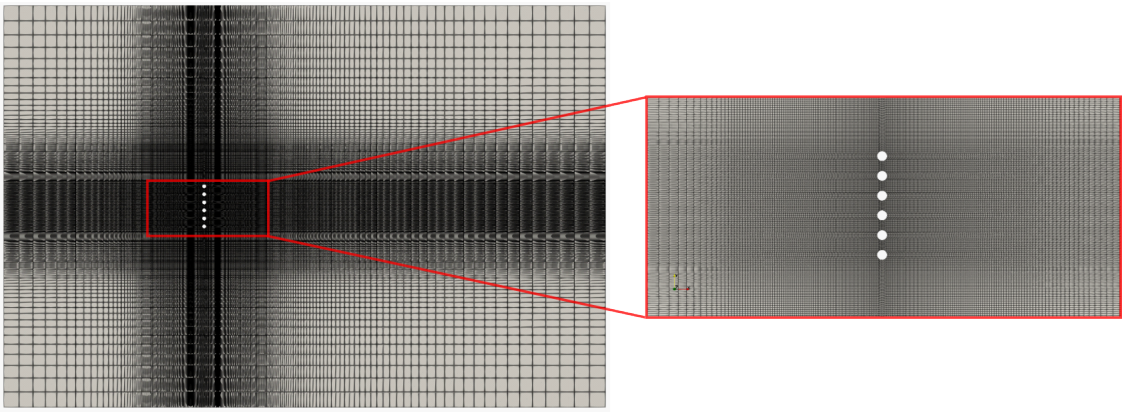

Figure 10: Computational Mesh for 6 bristled wing at 90°AOA

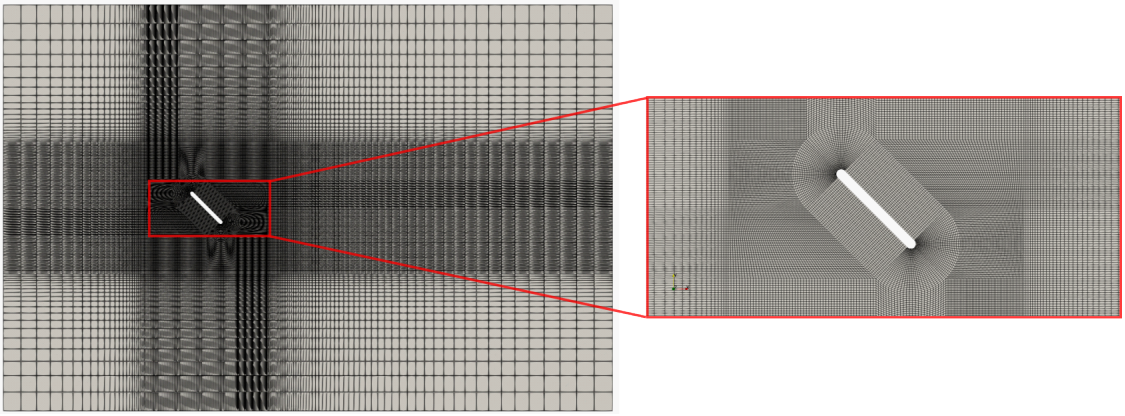

Figure 11: Computational Mesh for solid wing at 45°AOA

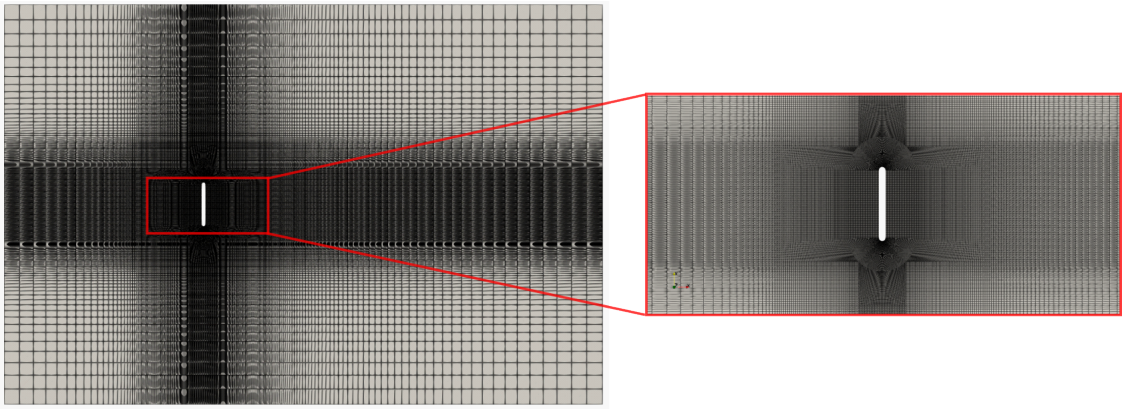

Figure 12: Computational Mesh for solid wing at 90°AOA

2.4.0.1 Fluid Properties

For this study, a theoretical fluid is utilized. To obtain a Reynolds number (Re) of 30 based on chord length, with a constant inlet velocity of 1 m/s, the kinematic viscosity (ν) is adjusted while maintaining a constant chord length (L) of 1 m. The formula for calculating Reynolds Number (Re) is given as:

$$Re = \frac{UL}{\nu} \tag{3}$$

where U is the free-stream inlet velocity, L is the chord length and ν is the kinematic viscosity. Hence, the calculated kinematic viscosity (ν) is 0.033 m^2/s. Reynolds number based on bristle diameter (Re_b) is given as:

$$Re_b = \frac{UD}{\nu} \tag{4}$$

where D is the bristle diameter and the corresponding Reynolds number based on bristle diameter (Re_b) is 3.

2.4.0.2 Porosity

The porosity of the model wing is defined as the ratio of the area occupied by the bristles to the area of an equivalent solid wing.

$$Porosity = \frac{A_{bristles}}{A_{solid}} \tag{5}$$

where $A_{bristles}$ is the total area occupied by the bristles in model bristle wing and A_{solid} is the total area of an equivalent solid wing.

2.4.0.3 Dimensionless Forces

In order to compare the forces from the numerical simulation, instantaneous forces experienced by the model wing were non-dimensionalized by $0.5\rho U^2 L$. C_l and C_d denote the lift and drag coefficients, respectively.

2.4.0.4 Initial and Boundary Conditions

Four boundaries (inlet, outlet, walls and wing) are defined in the blockMeshDict file. The initial and boundary conditions are shown in Table 2, 3 and 4.

Table 2: Initial Conditions

Flow Variable	Value
U	$0\ m/s$
p	$0\ m^2/s^2$

Table 3: Boundary Condition for p

Patch	Condition	Value (m^2/s^2)
inlet	zeroGradient	-
outlet	fixedValue	0
walls	zeroGradient	-
wing	zeroGradient	-
defaultFaces	empty	-

Table 4: Boundary Condition for U

Patch	Condition	Value (m/s)
inlet	fixedValue	(1, 0, 0)
outlet	zeroGradient	-
walls	slip	-
wing	noSlip	-
defaultFaces	empty	-

2.4.0.5 Equation Discretization

In OpenFOAM, Finite Volume Method (FVM) is used to discretize and solve the continuum equations. After mesh generation, the NS equation given in equation (1, 2) are to be solved on those individual cells. This is generally composed of temporal, spatial and equation schemes.

Equation discretization defines the computational methods used on the conservation laws for a specific time-step and location, described by the temporal and spatial discretization. The discretization schemes used in this study is given in Table 5.

Table 5: Discretization Schemes

Discretization	Scheme	Order of accuracy
Temporal	Euler	First
Gradient	Gauss linear	Second
Laplacian	Gauss linear corrected	Second
Interpolation	Linear	Second

2.4.0.6 Solution Method and Control

The solvers used in the study is shown in Table 6. For PIMPLE algorithm, two correction steps are used within a single time-step and does not utilize any non-orthogonal correctors. A flow time step of 1e-4 has been chosen for the simulation. .

Table 6: Numerical Solvers

Field	Linear Solver	Smoother	Tolerance
p	GAMG Solver	DIC Gauss Seidel Smoother	1e-6
U	Smooth Solver	Symmetric Gauss Seidel Smoother	1e-5

3 Results and Discussions

3.1 Grid Size Convergence Test

3.1.1 Bristle Wing

Four mesh sizing were taken for grid size convergence study. Coefficient of drag (C_d) and coefficient of lift (C_l) over the wing model was selected as the convergence test parameter.

Richardson extrapolation method given by Roache [9] is used to calculate the exact value of C_d and C_l taking the three most refined cases. This method calculates the exact value of the test parameter as the grid spacing tends to 0 (i.e. $\Delta x \rightarrow 0$ and $\Delta y \rightarrow 0$).

The constant grid refinement ration (r) is approximately set to 2.

The result of grid convergence test is shown in Table 7 and 8.

The exact value of coefficient of drag (C_d) and lift (C_l) obtained was 1.72512 and 0.770488 respectively. Taking the factor of safety value as 1.5, the calculated Grid Convergence Index (GCI) is given in Table 9.

Table 7: Grid Convergence Study using C_d

Grid level	Number of Elements	Coefficient of drag (C_d)	Error	Error (%)
M1	16774	1.71857	0.00655	0.379684
M2	35629	1.72277	0.00235	0.136222
M3	73705	1.72497	0.00015	0.008695
M4	145564	1.72511	0.00001	0.00058
Richardson Extrapolation	-	1.72512	-	-

Table 8: Grid Convergence Study using C_l

Grid level	Number of Elements	Coefficient of lift (C_l)	Error	Error (%)
M1	16774	0.72801	0.042478	5.513129
M2	35629	0.75116	0.019328	2.50854
M3	73705	0.76392	0.006568	0.852447
M4	145564	0.7682	0.002288	0.296955
Richardson Extrapolation	-	0.770488	-	-

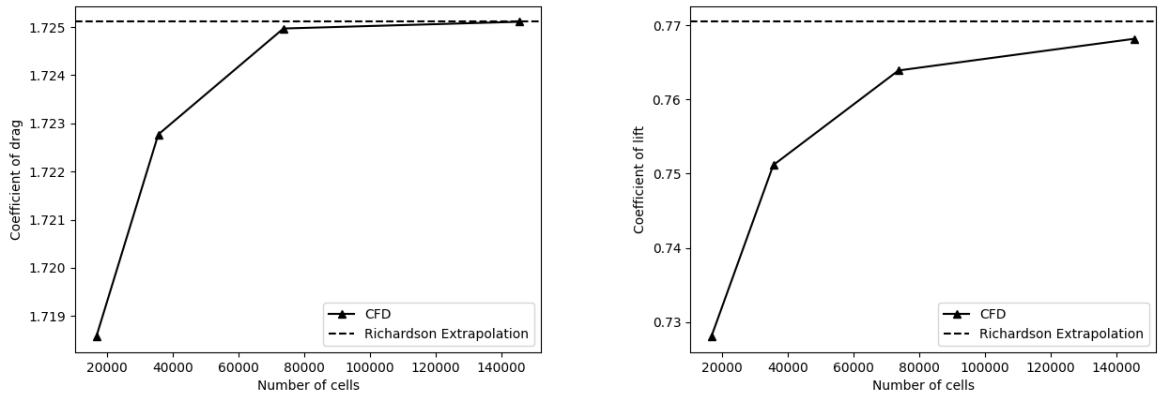

(a) Coefficient of Drag (C_d)

(b) Coefficient of Lift (C_l)

Figure 13: Richardson Extrapolation for 5 Bristle Wing Model

Table 9: Grid Convergence Index

	Coefficient of drag (C_d)	Coefficient of lift (C_l)
Coarse to Medium	0.011%	1.116%
Medium to Fine	0.0008%	0.4136%

Table 10: Converged Mesh's Parameters for Bristled wing

	Min $\Delta x(m)$	Max $\Delta x(m)$	Min $\Delta y(m)$	Max $\Delta x(m)$
Inside Bounding Box	0.0101	0.0101	0.0101	0.0101
Outside Bounding Box	0.0101	0.1467	0.0101	0.14

The M3 mesh is assumed to be converged as it is within the asymptotic range of convergence and is taken for further study. The converged mesh's parameters are tabulated in Table 10. The mesh consists of 73705 total cells. The maximum skewness of the mesh is 0.5491 with a maximum non-orthogonality of 38.45°.

3.1.2 Solid Wing

Similar approach was taken for studying the grid convergence for solid wing as well. The results of grid convergence study for solid wing is given in Table 11 and 12.

Table 11: Grid Convergence Study using C_d

Grid level	Number of Elements	Coefficient of drag (C_d)	Error	Error (%)
M1	10752	1.72667	0.02237	1.27899
M2	22145	1.73706	0.01198	0.68495
M3	43608	1.74205	0.00699	0.39965
M4	86740	1.74498	0.00406	0.23213
Richardson Extrapolation	-	1.74904	-	-

Table 12: Grid Convergence Study using C_l

Grid level	Number of Elements	Coefficient of lift (C_l)	Error	Error (%)
M1	10752	1.14776	0.01384	1.19146
M2	22145	1.15313	0.00847	0.72197
M3	43608	1.15609	0.00551	0.47435
M4	86740	1.15803	0.00357	0.30733
Richardson Extrapolation	-	1.1616	-	-

The calculated GCI is shown in Table 13.

Figure 14 shows the grid convergence plots for solid wing.

Table 13: Grid Convergence Index

	Coefficient of drag (C_d)	Coefficient of lift (C_l)
Coarse to Medium	0.4959%	0.5885%
Medium to Fine	0.2852%	0.3782%

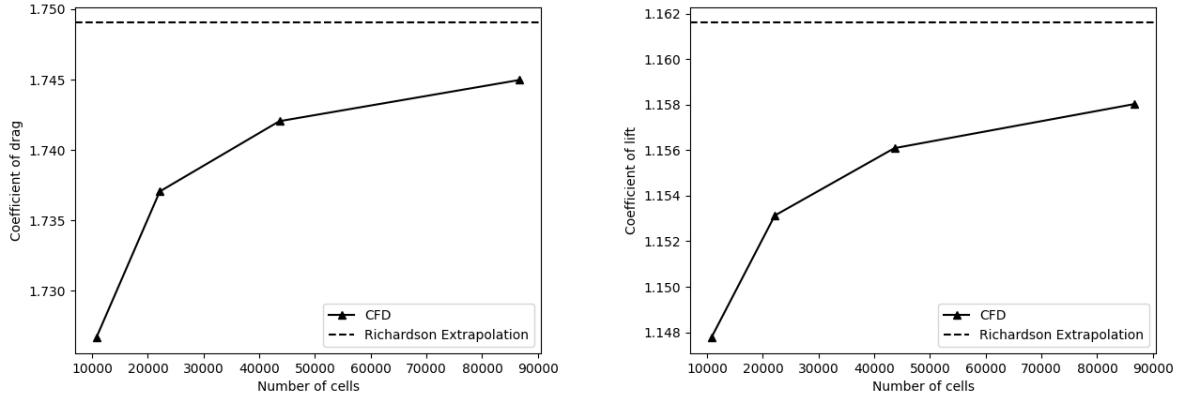

(a) Coefficient of Drag (C_d)

(b) Coefficient of Lift (C_l)

Figure 14: Richardson Extrapolation for Solid Wing Model

The M3 mesh is assumed to be converged as it is within the asymptotic range of convergence and is taken for further study. The converged mesh's parameters are tabulated in Table 14. The mesh consists of 43608 total cells. The maximum skewness of the mesh is 0.6559 with a maximum non-orthogonality of 44.728°.

Table 14: Converged Mesh's Parameters for Bristled wing

	Min $\Delta x(m)$	Max $\Delta x(m)$	Min $\Delta y(m)$	Max $\Delta x(m)$
Inside Bounding Box	0.02828	0.02828	0.02828	0.02828
Outside Bounding Box	0.02828	0.46	0.02828	0.46

3.2 Results

3.2.1 Aerodynamic Forces at $\alpha = 90°$

For comparing the forces between the model wings, the non-dimensional drag or drag coefficient (C_d) and the non-dimensional lift or lift coefficient (C_l) are defined. The computed drag coefficients for wing model at 90°AOA is shown in Figure 15 and the values are given in Table 15. Figure 16 shows velocity contour with streamlines pattern around the wing.

The solid wing has the highest value of C_d of 2.44599. The two weak counter-rotating vertices at the back of the solid wing can be seen on Figure 16. This vertices are formed due to the flow

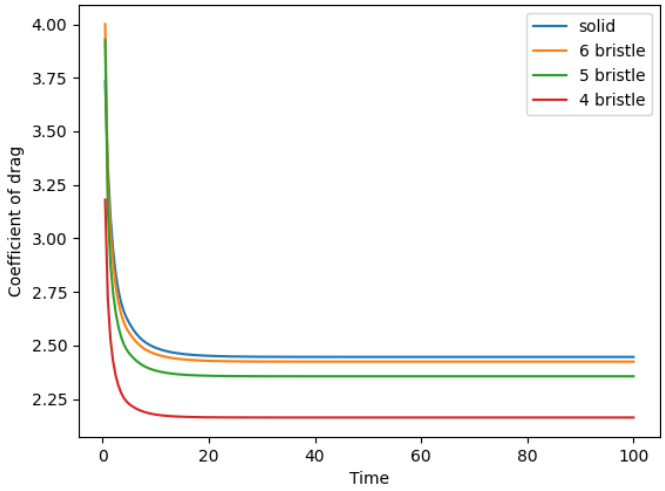

Figure 15: Coefficient of drag at 90°AOA

Table 15: Drag Coefficients of the model wings at 90°AOA

	Solid wing	Six-bristle wing	Five-bristle wing	Four-bristle wing
C_d	2.44599	2.42401	2.35547	2.16304

separation occurred at leading and trailing edges of the wing. This creates positive pressure in the front surface of the solid wing and the two vortices on the back give the negative pressure on the back surface. Hence large drag is experienced for solid wing model.

For six-bristle wing model, it is seen that the size of vortex behind the wing is smaller than that of the solid wing which significantly reduces for five-bristle wing and finally vanishes for four-bristle wing model. The result also shows that the value of C_d decreases as the number of bristles decreases. For 4-bristle wing model, C_d is 2.16304 which is lowest among all. The obtained C_d for model wing with 6 and 5 number of bristles are 2.42401 and 2.35547 respectively.

Vorticity contour for all the model wings are shown in Figure 17, where the blue and red color indicate the clockwise and counter-clockwise direction respectively. The two counter-rotating vortices can be seen in Figure 17a for solid wing. For bristle wing, each individual bristle operates within a creeping flow regime, as noted by Rajani et al. [10] for Re_b of 3. This results in the formation of strong shear layers around each bristle, preventing flow separation. The vorticity within the gaps between bristles is annihilated by vorticity of opposite sign generated by adjacent bristles due to strong viscous diffusion. Thus, the vorticity in the gaps is weaker than the vorticity at the outer edges of the wing (Figure 17b, 17c and 17d). The size and magnitude of the outer-edge vortices of the 6-bristled wing are comparable to those of the solid wing shown in Figure 17a. Thus 6-bristled wing experience nearly equal drag force than that of solid wing.

As the number of bristles decreases, the gap width increases which decreases the interference effect as can be seen in Figure 17c and 17d. Hence lower drag is experience by 4-bristled wing as more flow can pass through the gap.

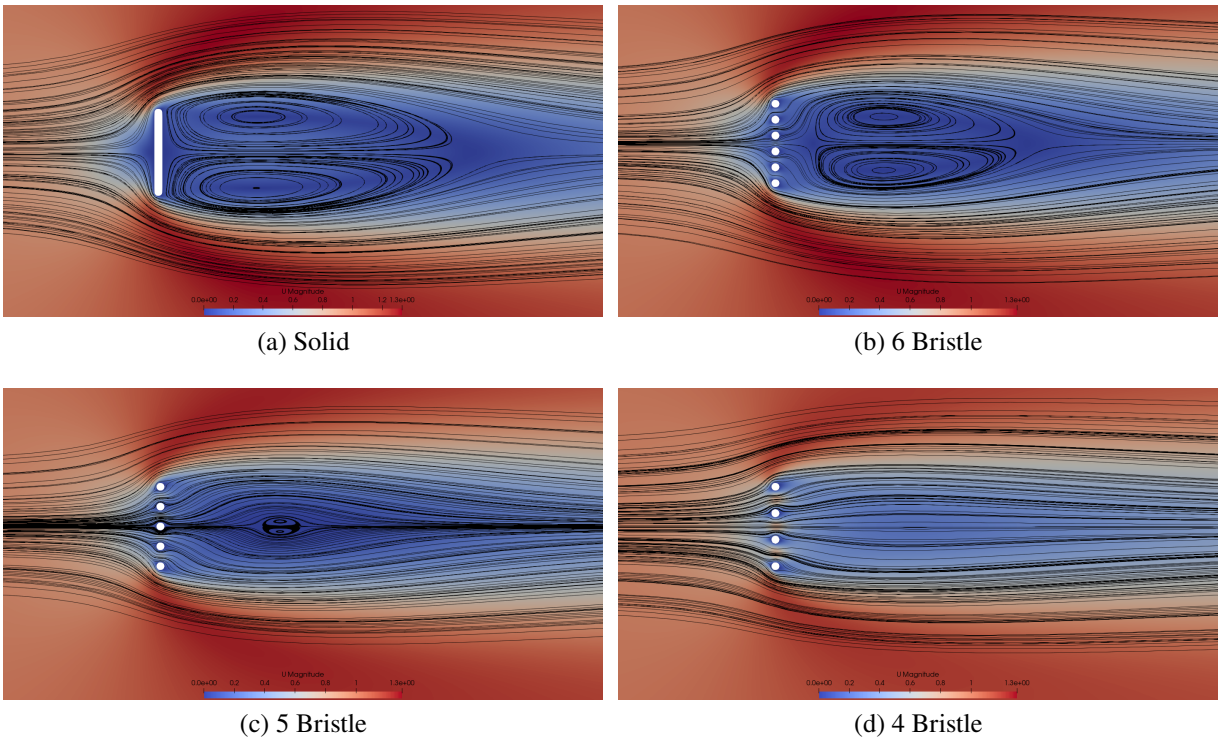

(a) Solid (b) 6 Bristle

(c) 5 Bristle (d) 4 Bristle

Figure 16: Velocity Contour with streamlines at 90°AOA

3.2.2 Effect of Angle of Attack

In the study on flow dynamics between gill rakers [11], the authors found that the velocity and angle of attack of the flow are crucial in forming vortices. These vortices reduce the effective gap size between the rakers, thereby altering the leakiness. In the study conducted by Jones et. al. [12], similar variation in leakiness with changes in the angle of attack was observed when the bristle wing was translated at 45°angle of attack. They found that the magnitude of force coefficients decreased with decreasing the number of bristles. The magnitude of this effect was greatest for lift at angles of attack near 45°, and for drag at angles of attack approaching 90°. This nature has already been discussed for drag at 90°AOA.

Vorticity contour and velocity streamlines for wings at 45°AOA are shown in Figure 18 and 19 respectively.

For solid wing, all the fluid flows around the outermost edges of the wing as the fluid cannot penetrate the wing surface. Therefore, the leading edge vortex of the solid wing is more strongly developed. However, for bristle wing model, each bristle generates a pair of counter-rotating vortices. These vortices exhibit greater size and magnitude near both the leading and trailing edges of the wing. At an angle of attack of 45°, vortices disperse more widely, covering a larger area. This dispersion effectively diminishes the gap between the bristles, which alters the interference effect and the volume of fluid passing through the gap between the bristles.

Observing the streamline pattern, it can be seen that more fluid is able to pass through the gap near the leading edge that the gap near trailing edge. This is due to change in effective length near trailing edge due to the superimposition of the shear layer. Thus large separation region near

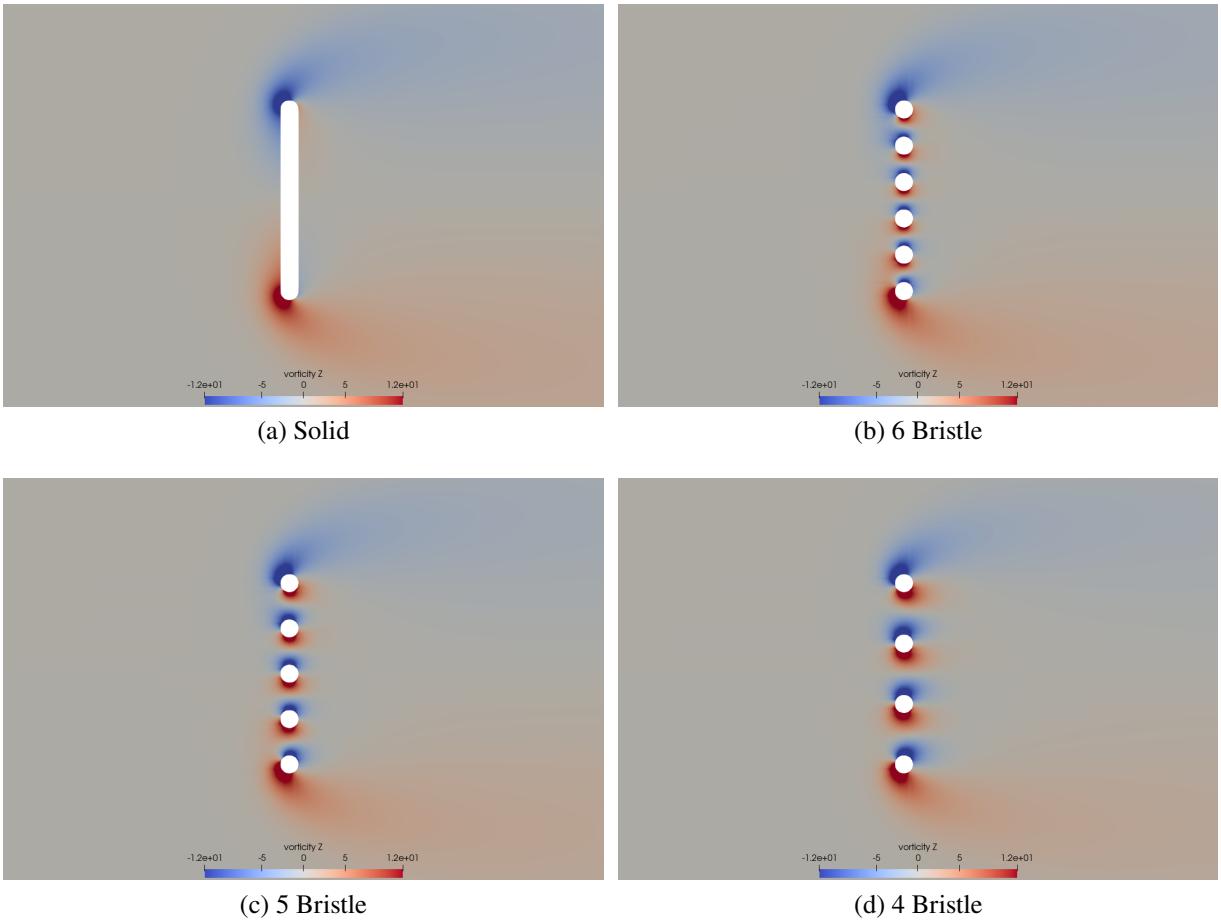

(a) Solid (b) 6 Bristle

(c) 5 Bristle (d) 4 Bristle

Figure 17: Vorticity contour at 90°AOA

trailing edge can be seen behind the 6-bristled wing model (Figure 19b). As the number of bristle decreases, it can be seen that the interference effect decreases and more fluid is able to pass through the gap even at 45°AOA. This explains the larger lift to drag ratio for 6-bristled wing model than that of 4-bristled wing model.

Figure 20 shows the force coefficients comparison for all the model wings obtained from simulation. The obtained value of C_d and C_l with their corresponding C_l/C_d are given in Table 16.

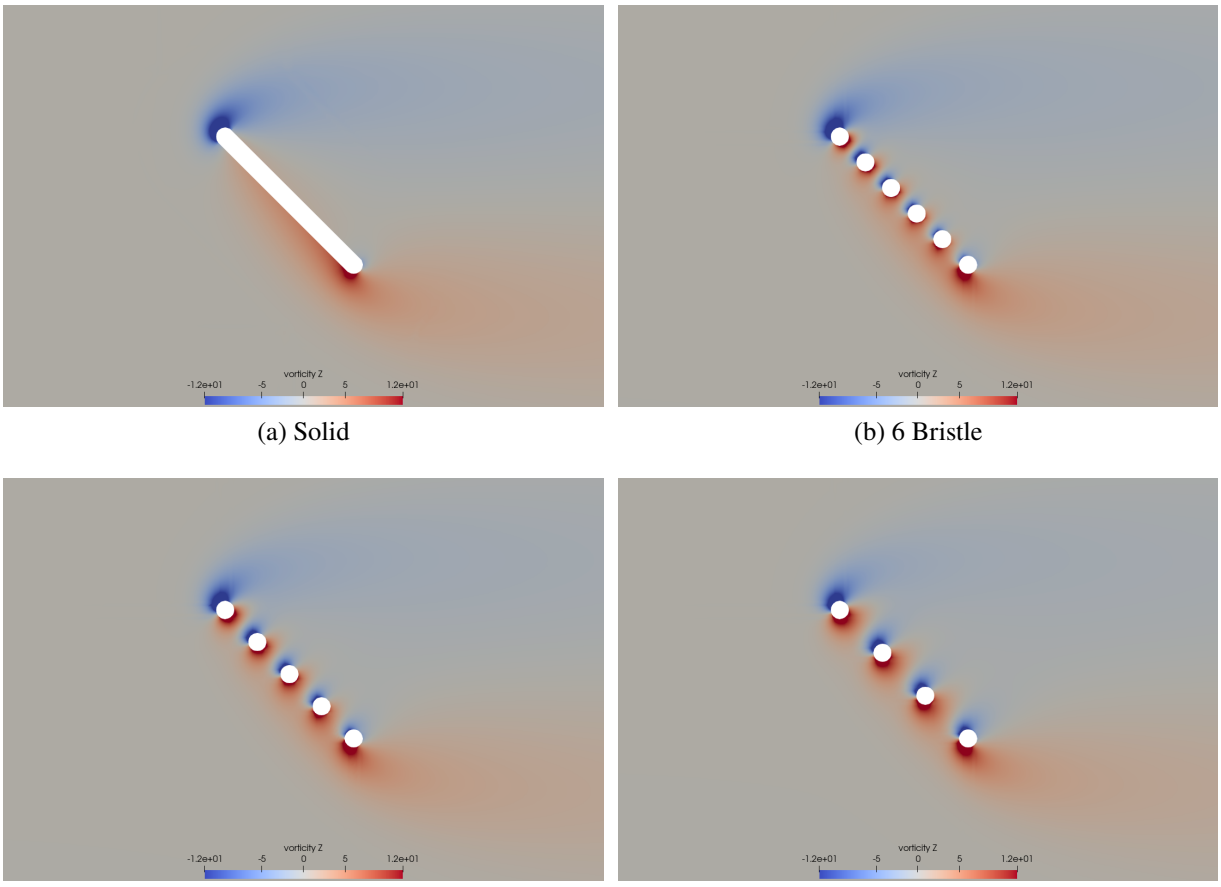

(a) Solid (b) 6 Bristle

(c) 5 Bristle (d) 4 Bristle

Figure 18: Vorticity Contour

Table 16: Computed values of C_d and C_l

	Coefficient of drag (C_d)	Coefficient of lift (C_l)	C_l/C_d
Solid Wing	1.74205	1.15609	0.6636
6 Bristle	1.74912	0.96341	0.5508
5 Bristle	1.72497	0.76392	0.4429
4 Bristle	1.65446	0.43698	0.2641

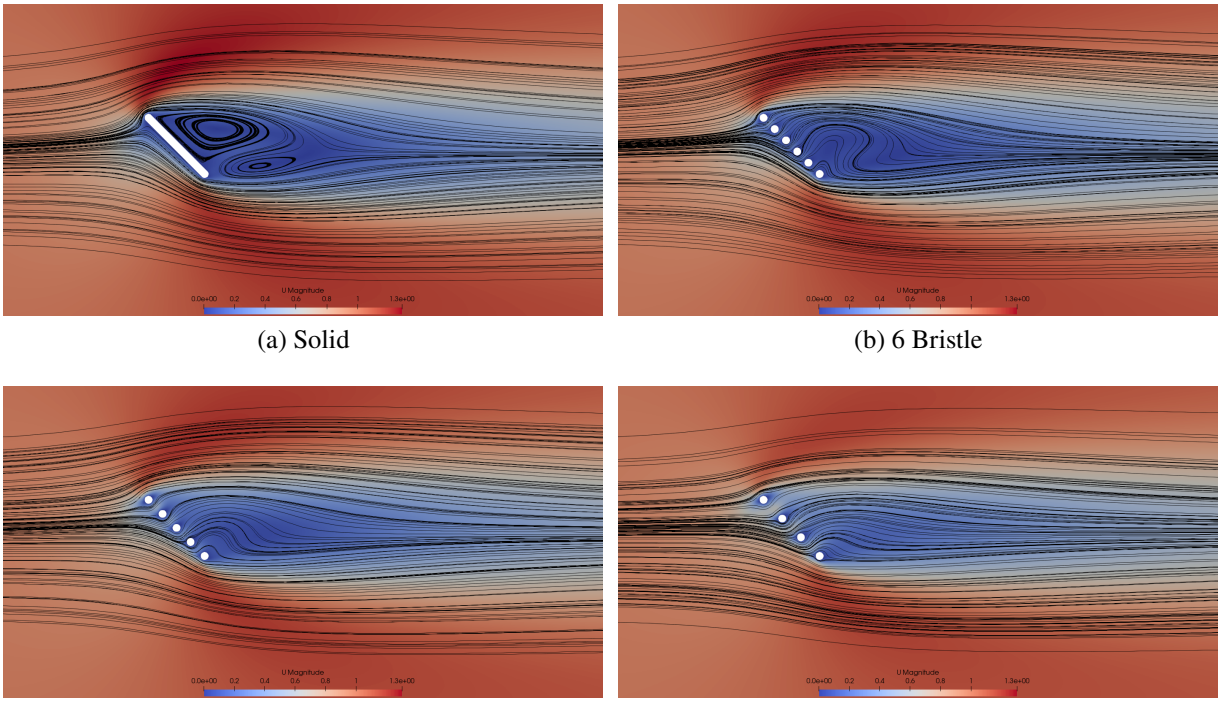

(a) Solid (b) 6 Bristle

(c) 5 Bristle (d) 4 Bristle

Figure 19: Velocity Contour with streamlines at 45°AOA

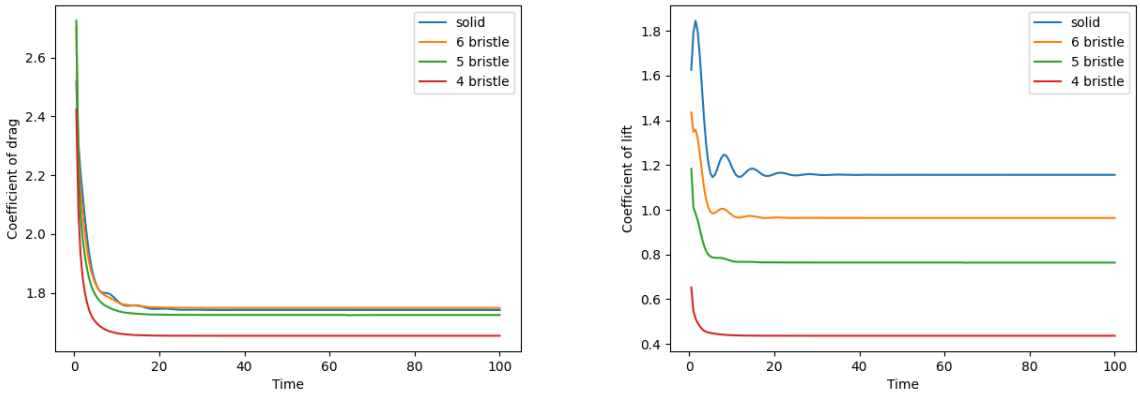

(a) Coefficient of drag (C_d) (b) Coefficient of lift (C_l)

Figure 20: Comparison of force coefficients

4 Conclusions

In conclusion, the aerodynamic analysis at 90° angle of attack (AOA) demonstrates that the drag coefficient (C_d) decreases with the reduction in the number of bristles in the wing model, with the solid wing exhibiting the highest drag coefficient of 2.44599 and the four-bristle wing, the lowest at 2.16304. The streamlines and vorticity contours reveal that the solid wing generates larger counter-rotating vortices due to flow separation at the leading and trailing edges, resulting in significant drag. In contrast, bristle wings, particularly the four-bristled wing model, experience less flow separation and interference effects, allowing more fluid to pass through the gaps and reducing drag. At 45° AOA, although all models show a reduction in C_d compared to 90° AOA, the lift-to-drag ratio (C_l/C_d) varies, with the solid wing having a ratio of 0.6636, while the four-bristle wing has the lowest ratio of 0.2641. These results suggest that bristle wings are more aerodynamically efficient at high AOAs, particularly in terms of reducing drag. The 2D transient laminar simulations for both solid and bristled wing models at a low Reynolds number of 30 were completed using OpenFOAM v2112. However, the validation of the simulation setup and results has not yet been completed.

5 Acknowledgement

I would like to extend my heartfelt gratitude and admiration to Prof. Chandan Bose of the University of Birmingham for his unwavering support and guidance throughout my internship project. Additionally, I deeply appreciate Prof. Janani Muralidharan for her valuable insights during our weekly review meetings. I am also grateful to Mr. Harish Jayaraj for assisting me with any challenges and questions I encountered during this period. Lastly, I want to express my gratitude to Ms. Payel Mukherjee and the FOSSEE team at IIT Bombay for their support and for providing me with this valuable internship opportunity.

References

[1] A. Santhanakrishnan, S. K. Jones, W. B. Dickson, M. Peek, V. T. Kasoju, M. H. Dickinson, and L. A. Miller, "Flow structure and force generation on flapping wings at low reynolds numbers relevant to the flight of tiny insects," *Fluids*, vol. 3, no. 3, p. 45, 2018.

[2] S. H. Lee, M. Lahooti, and D. Kim, "Aerodynamic characteristics of unsteady gap flow in a bristled wing," *Physics of Fluids*, vol. 30, no. 7, 2018.

[3] S. H. Lee, M. Lee, and D. Kim, "Optimal configuration of a two-dimensional bristled wing," *Journal of Fluid Mechanics*, vol. 888, p. A23, 2020.

[4] S. H. Lee and D. Kim, "Aerodynamic response of a bristled wing in gusty flow," *Journal of Fluid Mechanics*, vol. 913, p. A4, 2021.

[5] Y. K. Wu, Y. P. Liu, and M. Sun, "Aerodynamics of two-dimensional bristled wings in low-reynolds-number flow," *AIP Advances*, vol. 11, no. 4, 2021.

[6] J. Huber and J. Noyes, "A new genus and species of fairyfly, tinkerbella nana (hymenoptera, mymaridae), with comments on its sister genus kikiki, and discussion on small size limits in arthropods," *Journal of Hymenoptera Research*, vol. 32, pp. 17–44, 2013.

[7] S. Sunada, H. Takashima, T. Hattori, K. Yasuda, and K. Kawachi, "Fluid-dynamic characteristics of a bristled wing," *Journal of experimental biology*, vol. 205, no. 17, pp. 2737–2744, 2002.

[8] S. H. Lee and D. Kim, "Aerodynamics of a translating comb-like plate inspired by a fairyfly wing," *Physics of fluids*, vol. 29, no. 8, 2017.

[9] P. J. Roache, "Quantification of uncertainty in computational fluid dynamics," *Annual review of fluid Mechanics*, vol. 29, no. 1, pp. 123–160, 1997.

[10] B. Rajani, A. Kandasamy, and S. Majumdar, "Numerical simulation of laminar flow past a circular cylinder," *Applied Mathematical Modelling*, vol. 33, no. 3, pp. 1228–1247, 2009.

[11] A. Cheer, S. Cheung, T.-C. Hung, R. H. Piedrahita, and S. L. Sanderson, "Computational fluid dynamics of fish gill rakers during crossflow filtration," *Bulletin of mathematical biology*, vol. 74, pp. 981–1000, 2012.

[12] S. K. Jones, Y. J. Yun, T. L. Hedrick, B. E. Griffith, and L. A. Miller, "Bristles reduce the force required to 'fling'wings apart in the smallest insects," *Journal of Experimental Biology*, vol. 219, no. 23, pp. 3759–3772, 2016.